Accepted Manuscript

Electrophoretic deposition and laser cladding of bioglass coating on Ti

Beijing Xue, Litong Guo, Xiaoyuan Chen, Yu Fan, Xuanru Ren, Baoe Li, Yihan Ling, Yinghuai Qiang

PII: S0925-8388(17)31001-0

DOI: 10.1016/j.jallcom.2017.03.209

Reference: JALCOM 41247

To appear in: *Journal of Alloys and Compounds*

Received Date: 29 November 2016

Revised Date: 9 March 2017

Accepted Date: 19 March 2017

Please cite this article as: B. Xue, L. Guo, X. Chen, Y. Fan, X. Ren, B. Li, Y. Ling, Y. Qiang, Electrophoretic deposition and laser cladding of bioglass coating on Ti, *Journal of Alloys and Compounds* (2017), doi: 10.1016/j.jallcom.2017.03.209.

Electrophoretic Deposition and Laser Cladding of Bioglass Coating on Ti

Beijing Xue[1], Litong Guo[1,2*], Xiaoyuan Chen[1], Yu Fan[1], Xuanru Ren, Baoe Li[3], Yihan Ling[1], Yinghuai Qiang[1]

[1] China University of Mining and Technology, Xuzhou 221116, P.R. China

[2]Australian Institute for Bioengineering and Nanotechnology, The University of Queensland, Brisbane, QLD 4072, Australia

[3] Hebei University of Technology, Tianjin 300130, P.R. China

Abstract: Bioglass coatings derived from electrophoretic deposition method were fused on Ti surface by laser cladding process using a continuous CO_2 laser. The specimens were studied by field-emission scanning electron microscopy, X-ray diffraction and bonding tests. Titanium oxide layer with hierarchical structures consisting of submicron rows of leaf-like embossments and nano-pores was obtained by combining acid etching and anodization processes, which increased the surface roughness of Ti. When heat-treatment temperature was 700 □ and high, $CaSiO_3$ phase began to crystallize from the bioglass matrix and the crystallinity reached its maximum at 700 ℃. During the electrophoretic deposition process, porous bioglass coatings composed of bioglass particles and fibers were deposited on Ti surface. Bioglass coatings with similar hierarchical structure containing submillimeter bioglass beads and microfibers were synthesized on Ti surface by laser fusion. There are no obvious microcracks at the interface of the Ti-coating, which revealed the good bonding between Ti-porcelain. With the laser scanning distance decreased, the bond strength increased accordingly. After only one day immersion in SBF, calcium phosphate began to

Corresponding author**:** Litong Guo, Ph.D., Professor, E-mail: guolitong810104@163.com. Tel: +86 516 83591979, Fax: +86 516 83591870.

precipitate on the bioglass coatings' surfaces. The thickness of the calcium phosphate precipitation and the amount of microparticles increased with immersion time.

Keywords: Biomaterials; Microstructure; Titanium; Laser processing; Electrophoretic deposition

1 Introduction

Titanium and its alloys were most used implant materials in orthopedic surgery because of their appropriate mechanical properties, good corrosion resistance, biocompatibility and low cost [1, 2]. However, their capability to adhere to bone tissue is unsatisfactory and may result in wear debris that can lead to inflammatory reactions [3]. Thus, in order to improve osseointegration and biocompatibility of medical implants, the titanium alloys are commonly coated with bioactive coatings. Consequently, the implant is able to establish a direct chemical bond with the surrounding bone tissue, resulting in increased lifespan inside the body [4].

Various techniques were developed to produce bioactive coatings such as magnetron sputtering [5], electrophoretic deposition [4, 6-8], laser deposition [9-12], sol–gel [13,14] and many other techniques. Among them, electrophoretic deposition (EPD) is a promising electrochemical technique for the creation of thin films with a control of the film morphology and thickness. The EPD process consists in the migration of bioceramic powder particles in suspension to form the coating at the surface of the implant under the effect of an electric field. However, the bonding strength between the coating and substrate is not high enough and the coating will gradually detach from the substrate after implanted into human body. Therefore, after deposition, post thermal treatments are normally needed to further densify the deposit and to improve the adhesion between the coating and

substrate.

Laser cladding has proved efficient in the fusion of a powder on a substrate and the laser energy melts the cladding material forming an excellent chemical and metallurgical bond with the substrate [15, 16]. This process allows for a layer by layer coating building on titanium substrates and may prevent unwanted phase changes in the titanium due to its limited heat affected zone and low dilution ratio [11]. During the laser cladding process, microstructure of the coating and the interface between the coating and the substrate has attracted greatest interest [16, 17]. Therefore, laser parameters were optimized to synthesize a crack-free coating on titanium. In addition, acid etching and anodization processes were combined to improve the surface roughness of Ti and chemical bonding between porcelain-Ti. The hydroxyapatite forming ability in SBF was further characterized considering the potential of the synthesized coatings as bone-contacting materials.

2 Experimental Procedures

2.1. Synthesis of Bioglass

The Bioglass having weight percent composition of (54%SiO_2–8%Na_2O–19%CaO–3%P_2O_5–7%K_2O-1%Li_2O-8%SnO) was prepared by conventional sol–gel process using Calcium nitrate tetrahydrate, sodium hydroxide, tetra ethylortho silicate (TEOS) and orthophosphoric acid as precursors [18]. The procedure involves mixing of tetra ethylortho silicate (TEOS) and ethanol, followed by nitric acid (HNO_3) for hydrolysis and stirred for 30 min to obtain the gel. The ratio of TEOS: HNO_3: ethanol: water is 1:0.5:0.25:4. After complete gelation, the following reagents were added in the interval of 30 min in theorder of sodium hydroxide, calcium nitrate and

orthophosphoric acid. The solution was stirred for 4 h to get a homogenous gel. Then the sol aged at 70℃for 24 h, and then sintered at 600, 700 and 800 ℃ for 4 h.

2.2 Anodization of titanium

ASTM grade II CP titanium was cast, ground and polished to prepare plate-shaped specimens (Φ13 mm × 0.5 mm). In a typical anodization process, the electrolyte was prepared by adding 0.3 wt% of ammonium fluoride (NH_4F, Sinopharm Chemical Reagent Co. Ltd., AR) and 1.25 vol% of distilled water into ethylene glycol ($C_2H_6O_2$, Sinopharm Chemical Reagent Co. Ltd., AR). In a typical preparation procedure, the titanium specimens (>99% purity, thickness of 0.5 mm) were pre-treated in 40 wt% HF acid, and then anodized in the electrolyte solution using a graphite counter electrode at 20V for 15 min at room temperature.

2.3 Electrophoretic deposition

In the EPD process, bioglasss powder suspensions (2 wt% solids) were prepared using distilled water as solvent. The pH of the suspensions was adjusted using hydrochloric acid solution (0.1 M). The EPD process was carried out using titanium substrate as cathode, employing a ITECH DC power IT6720 (ITECH Electronic Co., ltd). EPD was performed at constant voltage in the range 5-15 V at 25°C for 20 min.

2.4 Laser cladding of bioglass coatings

Laser cladding was carried out by using a LCY-400 (Wuhan Huagong Laser Technology Co., Ltd, China.) 400 W pulse CO_2 laser. The laser was operated by smart MC software with Argon as the feeding gas. The laser cladding parameters were selected as 100-200 W laser power, 120 HZ frequency, 0.3-0.5 mm beam diameter and 7.5-15 mm/s

traverse speed.

The surface roughness (R_a) of titanium was measured using a JB-4C surface roughness tester. The cross-section of the specimens were ground and polished successively. Microstructural characterization of laser-cladding coatings layers was observed by using a Jeol JSM6400 scanning electron microscope.

2.5 In-vitro Bioactivity test in SBF

The coated samples were immersed in 30 ml of SBF solution prepared according to the literature [18], and incubated at 37°C for 1, 3, 5, 7, 14, 30 days and the solution was refreshed every two days. Three samples for each condition and time point were assessed. After incubation, the specimens were removed, gently washed with deionized water for three times and dried at 37 ℃ before further characterization. The hydroxyapatite formation on the incubated samples was evaluated by SEM and Fourier Transform Infrared Spectroscopy (FTIR, Nicolet is5) in range of 4000-400 cm^{-1}.

3 Results and discussion

Figure 1 shows the FE-SEM photos of titanium surface anodized at 20 V for 15 min after pre-treatment in 40 wt% HF (a) lower magnification 50000× and (b) higher magnification 200000×. Hybrid structures with submicron rows of leaf-like embossments and nano-pores were synthesized after anodization of titanium at 20 V for 15 min with pre-treatment in 40 wt% HF, as shown in Fig. 1 (a) and (b). The formation of leaf-like embossment rows and nano-pores attributed to the hybrid effect of HF acid etching and anodization processes [3].

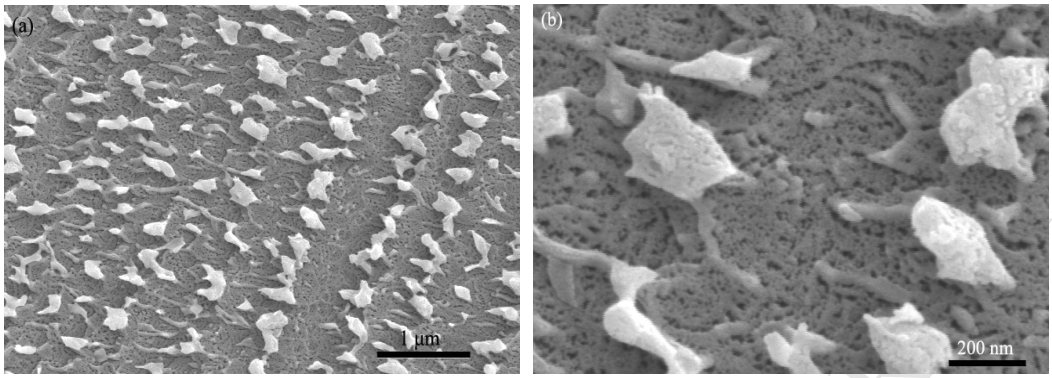

Fig. 1 FE-SEM photos of titanium surface anodized at 20 V for 15 min after pre-treatment in 40 wt% HF (a) lower magnification 50000× and (b) higher magnification 200000×.

The surface roughness of titanium was increased from 0.24±0.02 μm to 0.82±0.09 μm after anodization, which was mainly due to the existence of leaf-like embossments rows. In the previous research, the increased surface roughness of titanium increased the contact areas and mechanical bonding between titanium and coating [14]. In addition, anodization of titanium will help to increase the wettability between porcelain-Ti during laser fusion process. Therefore, the specimens were anodized with pre-treatment in HF acid in this study.

Figure 2 shows the XRD patterns of bioglass after heat-treatment at different temperature. The XRD results revealed that the major phase of the bioglass was $CaSiO_3$ [JCPDS 42-0550], whilst amorphous phase as secondary phase. When heat-treatment temperature was 600 □, the major phase of the bioglass was amorphous phase. When heat-treatment temperature was 700 □ and high, $CaSiO_3$ phase began to crystallize from the bioglass matrix and the crystallinity reached its maximum at 700 ℃. The formation of the $CaSiO_3$ phase will result in the good bioactive of the coating.

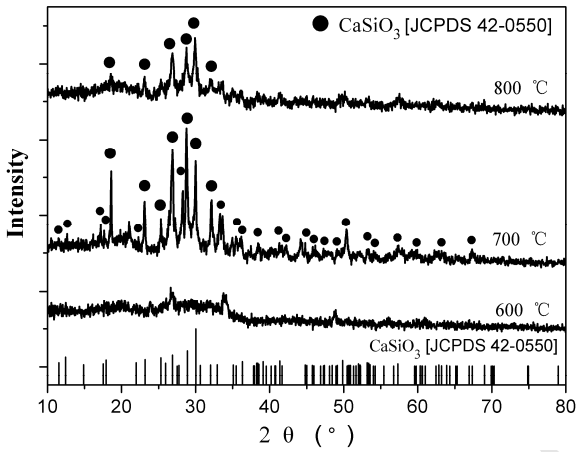

Figure 2 XRD patterns of bioglass after heat-treatment at different temperature.

Figure 3 shows the SEM microphotographs of the bioglass coatings on Ti synthesized by electrophoretic deposition. As shown in Fig. 3(a), a porous bioglass coating with some microcracks was deposited on titanium surface. The obtained bioglass coating was composed of bioglass particles (about 5-10 μm) and fibers (about 10-15 μm), as shown in Fig.3 (b). The formation of the micropores was attributed to the formation of hydrogen and oxygen during the electrophoretic deposition process.

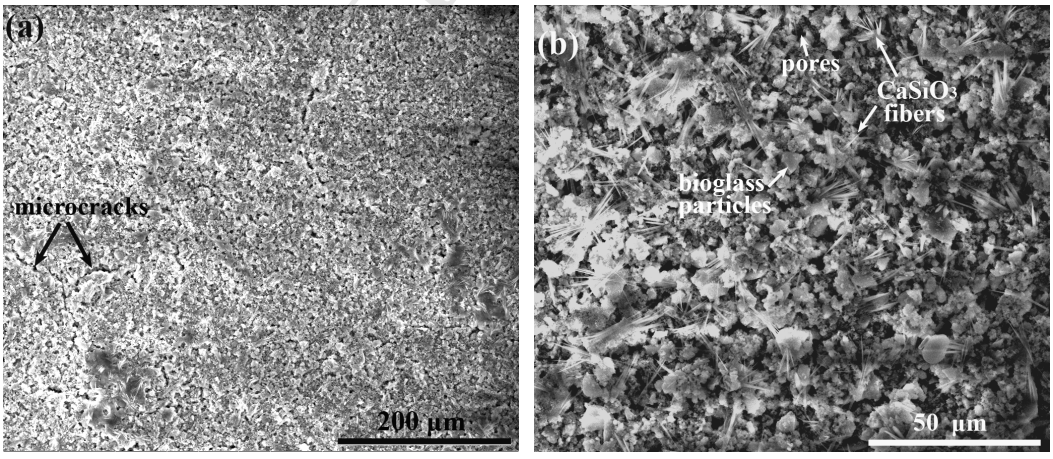

Figure 3 SEM microphotographs of the coatings on Ti by electrophoretic deposition.

Figure 4 shows the SEM microphotographs of the bioglass coatings on Ti synthesized

at different laser scanning distance (a), (b) 0.3 mm, (c), (d) 0.2 mm (e) and (f) 0.1 mm. Bioglass coatings with similar hierarchical structure containing submillimeter bioglass beads and microfibers were synthesized on Ti surface by laser fusion. The radii of the obtained bioglass beads were about 300-1000 μm, while the lengths of the microfibers were about 10-15 μm, as shown in Fig. 3. During the laser fusion process, the temperature field of the coating is inhomogeneous. The temperature at the center is higher than that at the edge of the laser scanning region. The bioglass at the center of the laser scanning region firstly reached its softening temperature point and formed the larger bioglass beads. In contrast, the smaller bioglass beads formed at the edge of the laser scanning region. With the laser scanning distance decreased, the sintering temperature increased accordingly and the temperature field of the coating became more homogeneous. The microcracks gradually healed and the amount of the microcracks decreased. In contrast, the amount of the microfibers increased accordingly.

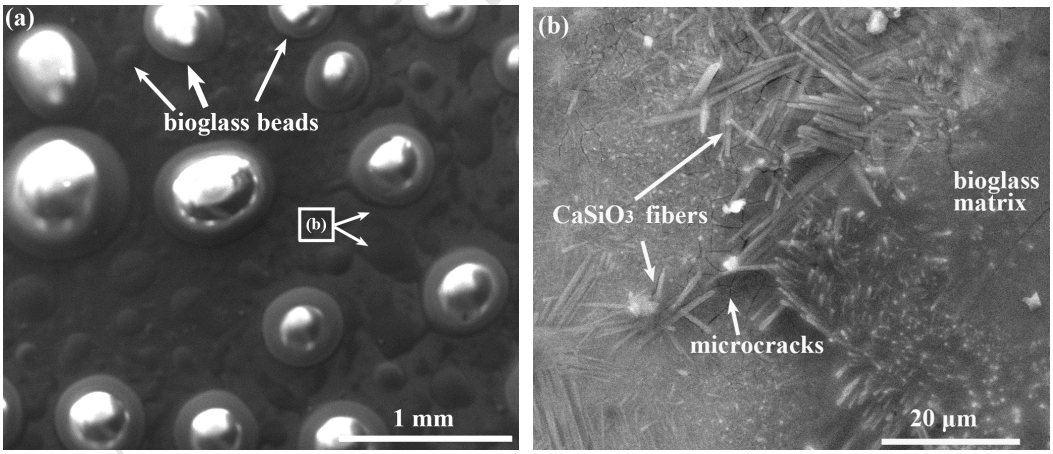

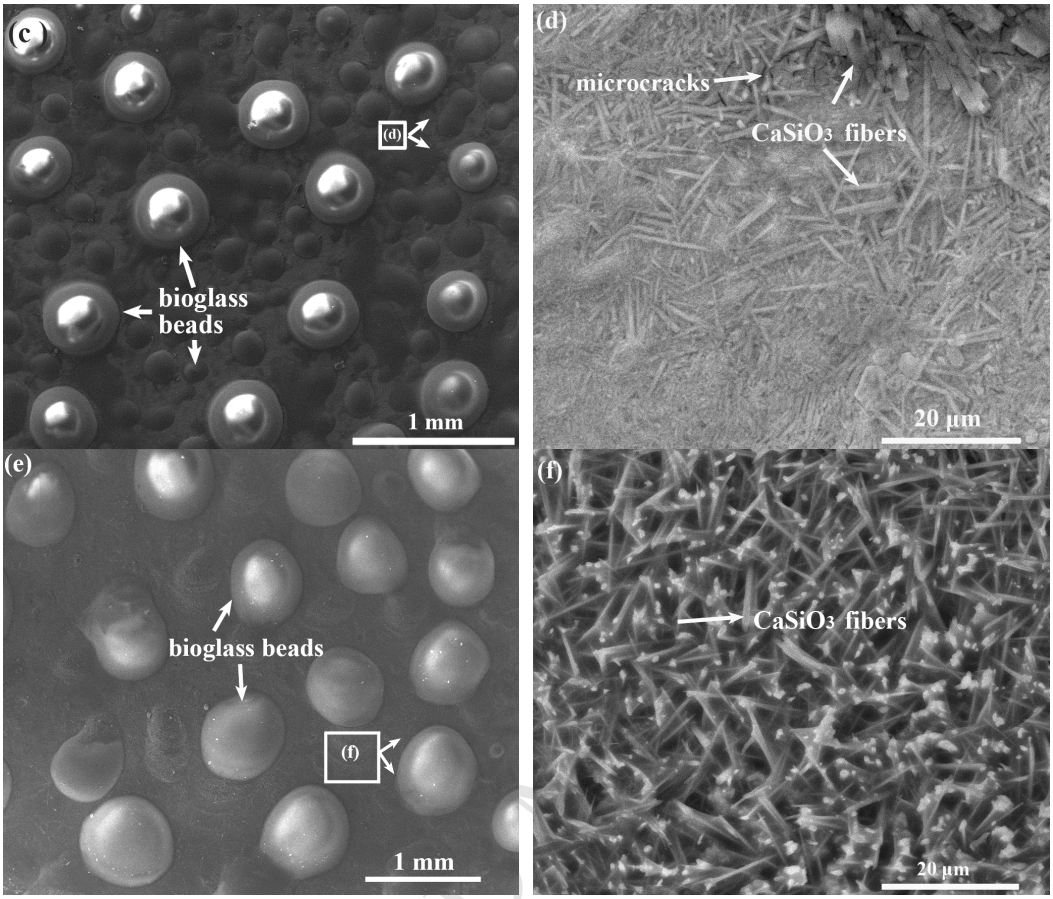

Figure 4 SEM microphotographs of the bioglass coatings synthesized at different laser scanning distance (a), (b) 0.3 mm, (c), (d) 0.2 mm, (e) and (f) 0.1 mm.

Figure 5 shows the SEM microphotographs of the cross-section of the bioglass coatings synthesized at different laser scanning distance (a) 0.3 mm, (b) 0.2 mm and (c) 0.1 mm. When the laser scanning distance was 0.3 mm, the height of the obtained bioglass beads was about 450 μm, while the size（radium）of the was about 1000μm. When the laser scanning distance was 0.2 mm and 0.1 mm, the heights of the obtained bioglass beads were about 450 μm and 120 μm, while the radii of the beads were about 450 μm and 120 μm, respectively. The height of the obtained bioglass beads decreased as the laser scanning

distance decreased, which revealed the increase of the wettability between the coating and Ti. In addition, for all the three specimens, there are no obvious microcracks at the interface of the Ti-coating, which revealed the good bonding between Ti-porcelain.

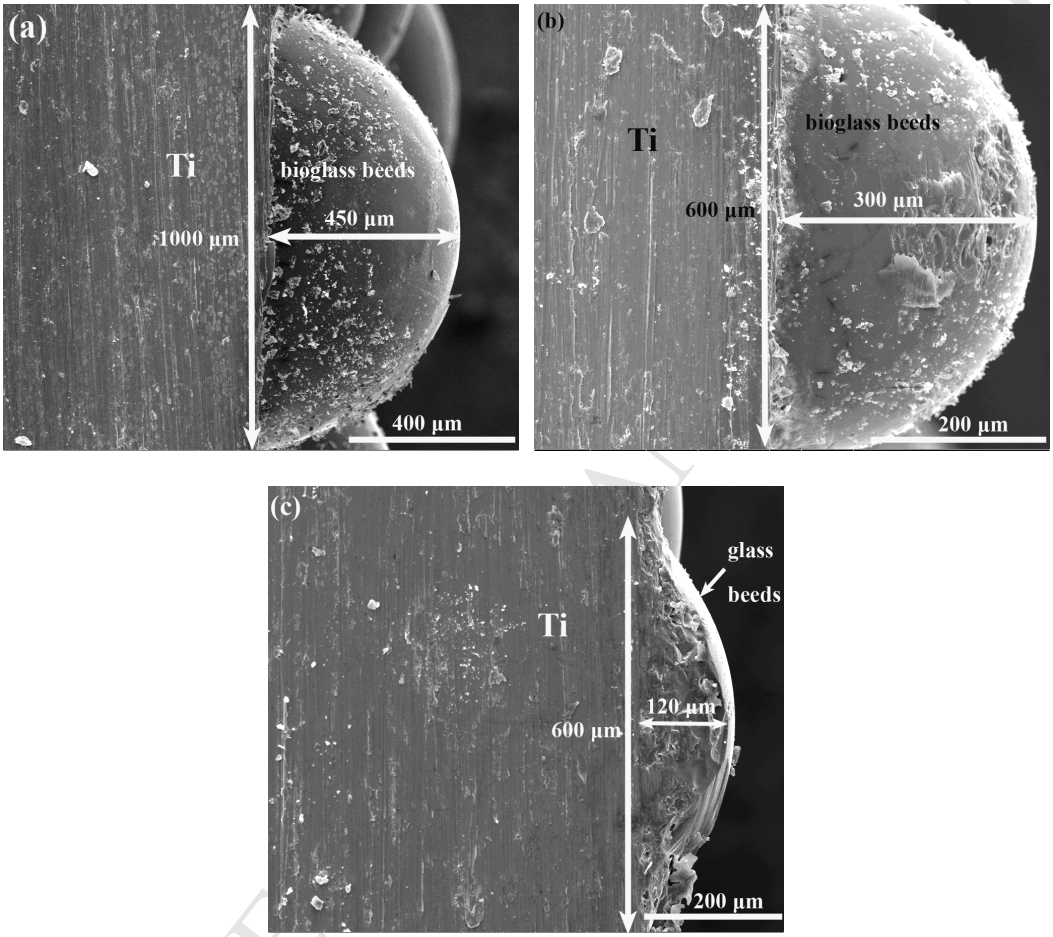

Figure 5 SEM microphotographs of the cross-section of the bioglass coatings synthesized at different laser scanning distance (a) 0.3 mm, (b) 0.2 mm and (c) 0.1 mm.

Then the tensile bond strength between porcelain-Ti was evaluated for the specimens after laser treatment at different scanning distance, as shown in table 1. With the laser scanning distance decreased, the bond strength increased accordingly. The increase of the bonding is due to the increase of the amount of fibers, improvement of wettability and interface quality between Ti-coating.

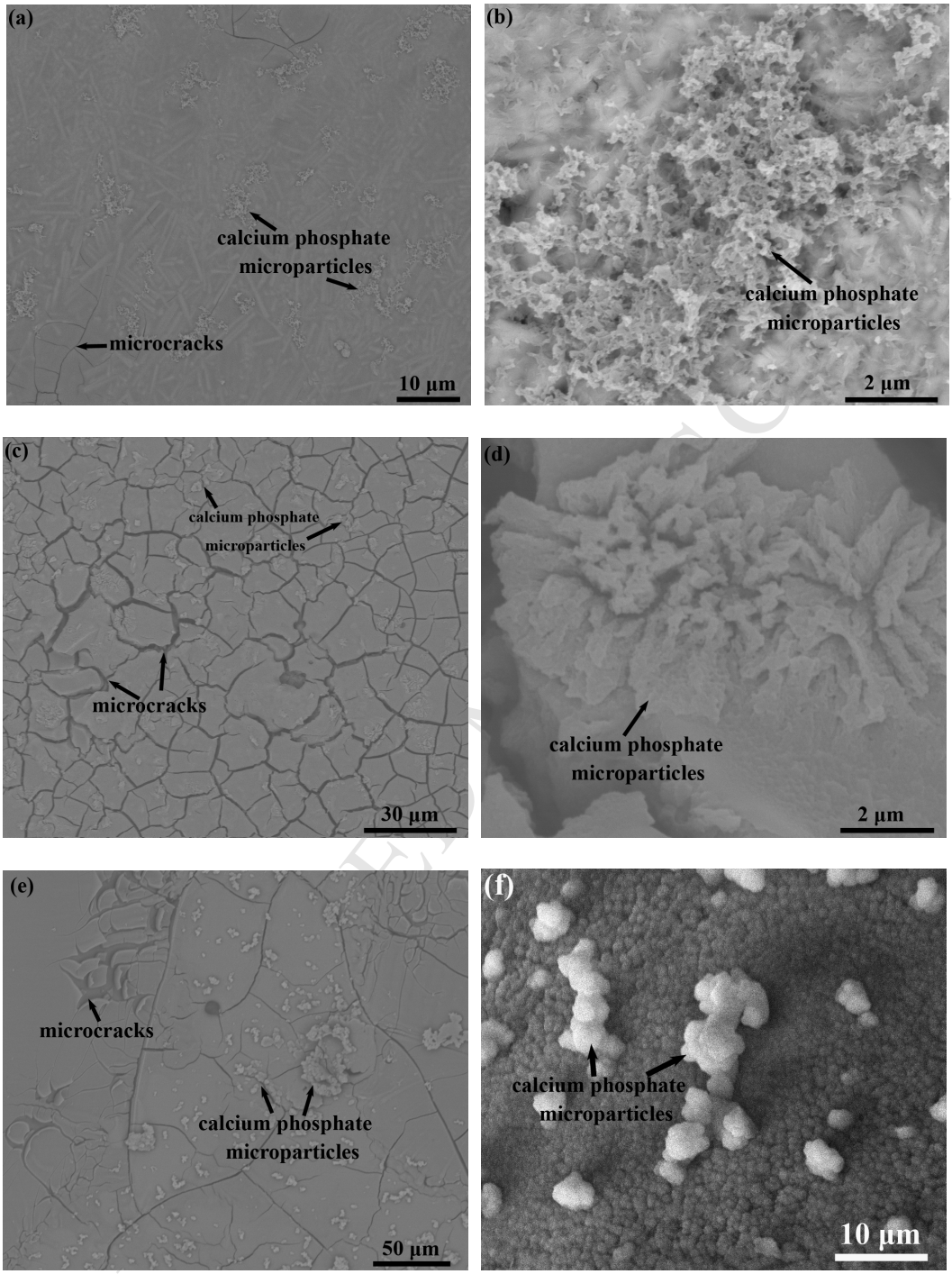
(a)
calcium phosphate microparticles
microcracks
10 µm
(b)
calcium phosphate microparticles
2 µm
(c)
calcium phosphate microparticles
microcracks
30 µm
(d)
calcium phosphate microparticles
2 µm
(e)
microcracks
calcium phosphate microparticles
50 µm
(f)
calcium phosphate microparticles
10 µm

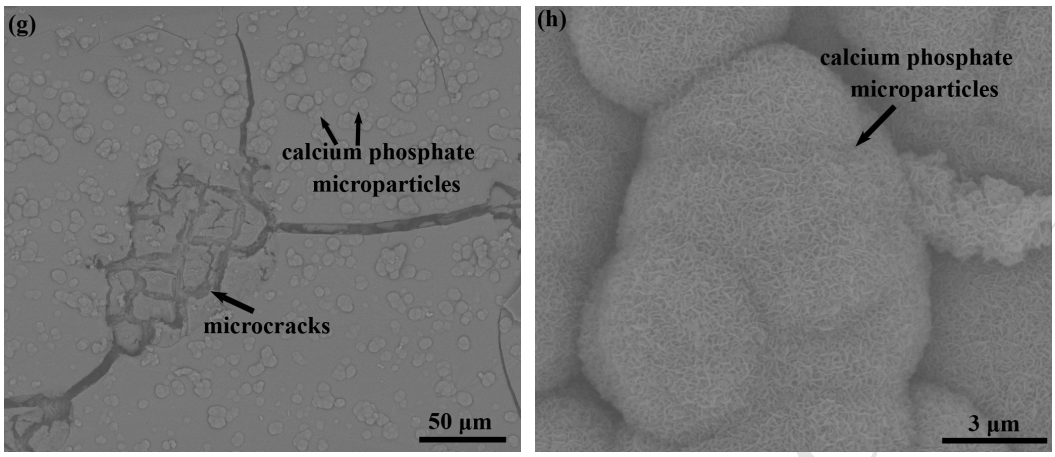

Figure 6 SEM microphotographs of calcium phosphate precipitates on the bioglass coatings at the different stage of immersion, (a), (b) 1 day; (c), (d) 3 days; (e) and (f) 7 days; the selected area was used for EDX analysis; (g) and (h) 14 days.

Figure 6 shows the SEM microphotographs of calcium phosphate precipitates on the bioglass coatings at the different stage of immersion, (a), (b) 1 day, (c), (d) 3 days, (e) and (f) 7 days, (g) and (h) 14 days. Fig. 6 (a) shows that after only one day immersion in SBF, calcium phosphate began to precipitate on the bioglass coatings' surfaces, but the precipitation layer was not thick enough to cover up the bioglass coating. Fig. 6 (b) shows that porous calcium phosphate microparticles were formed by the agglomeration of many nanoparticles (about 80nm). As shown in 6 (d), flowerlike microparticles were formed on the bioglass coating. In Fig. 6 (c), (e) and (g), it is clearly shown that the thickness of the calcium phosphate precipitation and the amount of microparticles increased with immersion time. While in Fig. 6 (d), (f) and (h), it is clearly shown that the calcium phosphate microparticles became denser with immersion time. As shown in 6 (h), calcium phosphate microparticles were formed by the agglomeration of wormlike particles (about 300nm) after 14 days immersion.

The SBF solution is highly supersaturated with respect to calcium phosphate, which leads to the spontaneous growth of the calcium phosphate after nucleation [18].

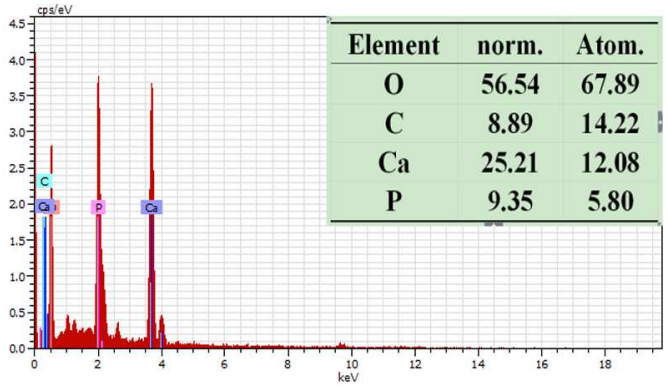

Element	norm.	Atom.
O	56.54	67.89
C	8.89	14.22
Ca	25.21	12.08
P	9.35	5.80

Fig. 7. EDX spectrum of the selected area in Fig. 6(f); the inset table shows the normalized weight and atomic ratios of the detected elements.

Surface EDX analysis was used to investigate the element composition of coating after 7 days incubation in SBF, as shown in Fig. 7. The EDX pattern of the selected area in Fig. 6 (f) revealed the presence of oxygen, calcium, carbon and phosphorus, which suggest the possible formation of carbonated hydroxyapatite which exhibits higher osteoconductive properties and earlier bioresorption compared to stoichiometric HA in vivo according to literature [18]. The weight and atomic ratios of detected elements are presented in the table in Fig. 7. The selected area had a Ca/P ratio of 2.08 which is higher than the value (1.67) of stoichiometric HA. Because some PO_4^{3-} was replaced by the CO_3^{2-} groups, the non-stoichiometric carbonated apatites are obtained, which had a higher Ca/P ratio than that of stoichiometric HA (1.67). Based on the experimental results of the in-vitro bioactivity test, it can be concluded that the coatings synthesized in this research are bioactive to be used as implant materials in the human body.

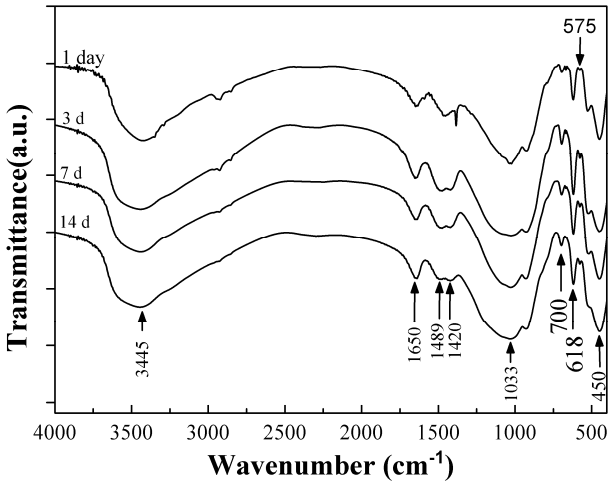

Figure 8 FTIR spectra of the bioglass coatings after different incubation time, 1 day, 3 days, 7 days and 14 days.

In the FTIR spectra, the characteristic bands in the region of 1650 to 1300 cm^{-1} (at 1420, 1489 and 1650 cm^{-1}) were due to C-O bending vibrations in the carbonate ions (CO_3^{2-}), while the characteristic peak at 700 cm^{-1} corresponded to the in-plane bending vibration of C=O in the carbonate ions. The characteristic peak at 1033 cm^{-1} corresponded to the stretching of PO_4^{3-} , while the characteristic bands in the region of 650 to 550 cm^{-1} (at 575 and 618 cm^{-1}) were attributed to the stretching vibration of the O-P-O in the PO_4^{3-} groups which occupied crystal lattice sites of the apatite, indicating the possible formation of CHA after 1 day of incubation. The split of the peaks in the range of 1400-1500 cm^{-1} referred to the formation of CHA. The rocking vibrational mode of Si-O-Si band at 450 cm^{-1}, standing for the presence of bioglass particles, is still visible after 14 days of incubation. The IR features at 3445 cm^{-1} indicated presence of remaining OH. These FTIR results supported the formation of carbonated hydroxyapatite in this study.

In the further work, pre-heating and other laser parameters optimizing will be employed

to reduce the excessive thermal stress at the interface of Ti-porcelain, so that to improve the bonding between the coating and Ti. In addition, the in vivo bioactivity of the coating will be characterized.

4 Conclusions

Titanium oxide layer with hierarchical structures consisting of submicron rows of leaf-like embossments and nano-pores was obtained by combining acid etching and anodization processes, which increased the surface roughness of Ti. When heat-treatment temperature was 700 ℃ and high, $CaSiO_3$ phase began to crystallize from the bioglass matrix and the crystallinity reached its maximum at 700 ℃. Bioglass coatings with similar hierarchical structure containing submillimeter bioglass beads and microfibers were synthesized on Ti surface by laser fusion. Larger bioglass beads formed at the center of the laser scanning region, while smaller bioglass beads formed at the edge of the laser scanning region. With the laser scanning distance decreased, the microcracks gradually healed and the amount of the microcracks decreased, which led to the increase of bond strength. After only one day immersion in SBF, calcium phosphate began to precipitate on the bioglass coatings' surfaces. The thickness of the calcium phosphate precipitation and the amount of microparticles increased with immersion time. The coatings synthesized in this research are bioactive to be used as implant materials in the human body.

Acknowledgements

This research was sponsored by the Natural Science Foundation of Jiangsu Province (No. BK20161182), QingLan Project of Jiangsu Province, and Fundamental Research Funds for the Central Universities (No. 2015XKMS064).

References

[1]. Guo LT, Tian JL, Wu J, Li B, Zhu YB, Xu C, Qiang YH, Effect of Nano-porous Film on the Bonding Strength of Titanium-Porcelain, Mater Lett, 2013; 109: 140-2.

[2]. Singh RK, Awasthi S, Dhayalan A, Ferreira JMF, Kannan S, Deposition, structure, physical and invitro characteristics of Ag-doped β -$Ca_3(PO_4)_2$/chitosan hybrid composite coatings on Titanium metal, Materials Science and Engineering C, 2016; 62: 692-701.

[3]. Guo LT, Chen XY, Liu XM, Feng W, Lin C, Li B, Qiang YH, Surface modifications and Nano-composite coatings to improve the bonding strength of titanium-porcelain, Mater Sci & Eng C, 2016; 61:143-8.

[4]. Mehralia M, Akhiani AR, Talebian S, Mehrali M, Latibari ST, Dolatshahi-Pirouz A, Metselaar HSC, Electrophoretic deposition of calcium silicate–reduced grapheme oxide composites on titanium substrate, Journal of the European Ceramic Society, 2016; 36(2), 319-32.

[5]. Ge F, Zhou X, Meng F, Xue Q, Huang F, Tribological behavior of VC/Ni multilayer coatings prepared by non-reactive magnetron sputtering, Tribiology Internat, 2016; 99: 140–50.

[6]. Alicja KK, Małgorzata KB, Grzegorz D, Anna DS, Elzbieta P, Wojciech S, Multilayer coatings formed on titanium alloy surfaces by plasma electrolytic oxidation-electrophoretic deposition methods, Electrochimica Acta, 2016; 204: 294-306.

[7]. Chen Q, Yang YY, Larraya UPD, Garmendia N, Virtanen S, Boccaccini AR. Electrophoretic co-deposition of cellulose nanocrystals-45S5 bioactive glass nanocomposite coatings on stainless steel, Applied Surface Science, 2016; 362: 323-8.

[8]. Zehbe R, Mochales C, Radzik D, Müller WD, Fleck C, Electrophoretic deposition of multilayered (cubic and tetragonalstabilized) zirconia ceramics for adapted crack deflection, Journal of the

European Ceramic Society, 2016; 36: 357-64.

[9]. Shishkovsky IV, Smurov I, Titanium base functional graded coating via 3D laser cladding, Mater Lett, 2012; 73: 32-5.

[10]. Li HC, Wang DG, Chen CZ, Weng F, Effect of CeO_2 and Y_2O_3 on microstructure, bioactivity anddegradability of laser cladding $CaO\text{-}SiO_2$ coating on titanium alloy, Colloids Surf B: Biointerfaces, 2015; 127: 15-21.

[11]. Diao YH, Zhang KM, Microstructure and corrosion resistance of TC2 Ti alloy by laser cladding with Ti/TiC/TiB2 powders, Appl Surf Sci, 2015; 352: 163-8.

[12]. Li M, Huang J, Zhu YY, Li ZG, Effect of heat input on the microstructure of in-situ synthesized TiN–TiB/Ti based composite coating by laser cladding, Surf & Coat Tech, 2012; 206(19-20): 4021-6.

[13]. Guo LT, Tian JL, Wu J, Li B, Zhu YB, Qiang YH, Sol-gel Synthesis of Hybrid Coating to Improve Titanium-Porcelain Bonding, Mater & Manu Proc, 2014; 29(9): 1025-9.

[14]. Guo LT, Feng W, Liu XM, Lin C, Li B, Qiang YH, Sol–gel synthesis of antibacterial hybrid coatings on titanium, Mater Lett, 2015; 160, 448-51

[15]. Wilson JM, Jones N, Jin L, Shin YC. 2013. Laser deposited coatings of Co-Cr-Mo onto Ti-6Al-4V and SS316L substrates for biomedical applications. J Biomed Mater Res B, 2013; 101B:1124–32.

[16]. Paydas H, Mertens A, Carrus R, Lecomte-Beckers J, Tchoufang Tchuindjang J, Laser cladding as repair technology for Ti–6Al–4V alloy: Influence of building strategy on microstructure and hardness, Mater & Design, 2015, 85: 497-510.

[17]. O'Flynn KP, Stanton KT, Laser sintering and crystallization of a bioactive glass-ceramic, J Non-Cryst Solid, 2013, 360: 49-56.

[18]. Naidu S, Scherer GW. Nucleation, Growth and Evolution of Calcium Phosphate Films on Calcite, Journal of Colloid and Interface Science, 2014, 435:128-137.

Table 1 Effect of laser scanning distance on the bonding strength between titanium-coating

scanning distance (mm)	bonding strength (MPa)
0.3	33.27±2.98
0.2	35.45±3.31
0.1	38.52±3.86

Prime Novelty Statement

(1) Bioglass coatings were fused on Ti surface by laser cladding process.

(2) Surface roughness of Ti was increased by surface modification of Ti.

(3) Apatite precipitated on the bioglass coatings after 1 day immersion.

(4) The thickness of the apatite precipitation increased with immersion time.